PCCP

PAPER

View Article Online
View Journal | View Issue

Cite this: *Phys. Chem. Chem. Phys.*, 2024, **26**, 12838

High-temperature molecular line list of hydroboron monoxide (HBO)†

Ximing Li, Zhi Qin * and Linhua Liu *

Received 9th December 2023,
Accepted 3rd April 2024

DOI: 10.1039/d3cp05997a

rsc.li/pccp

Hydroboron monoxide (HBO) is expected to occur in envelopes of the asymptotic giant branch (AGB), but a lack of spectroscopic data is hampering its possible detection. Using the state-of-the-art *ab initio* method, we present the first, comprehensive molecular line list for HBO which is suitable for temperatures up to T = 3000 K. This new line list covers the wavenumber range of 0–9000 cm^{-1} (wavelengths of $\lambda \geq 1.11$ μm), and it contains almost 75 million transitions between 435 631 energy levels with rotational excitation up to J = 120. The new line list of HBO can facilitate its future molecular detection in the laboratory and interstellar space.

1 Introduction

The light element, boron (B), is produced by the Big Bang nucleosynthesis, and its abundance in the atmosphere of young stellar objects is of special interest. The precise abundance of B is important for perfecting the standard Big Bang nucleosynthesis, determining the matter distribution and understanding the mixing processes in stars.[1–3]

In the envelopes of the asymptotic giant branch (AGB), most of the B element is predicted to be locked in the B-containing molecules. Concretely, the hydroboron monoxide (HBO) is predicted to be the main reservoir of B in S-, C-type atmospheres and O-rich atmospheres, and HBO is thought to be the main molecular carrier of the B element.[4] However, the elemental abundance of B is far lower than that of H, which has placed some constraints on the observation of the HBO basing spectroscopic data.[4] Thus, the spectroscopic information for HBO is expected to play an important role in determining the B abundance in AGB atmospheres.

Previous experimental studies[5–8] provided limited rovibrational spectroscopic data for the gas-phase hydroboron monoxide. The infrared spectrum of matrix-isolated isomer HBO was first observed by Lory and Porter.[8] In 1986, Kawashima *et al.*[7] reported the first gas-phase detection of HBO using discharge-modulated infrared spectroscopy and determined the infrared spectrum of the ν_3 band corresponding to the stretching vibration at 1826 cm^{-1}. In the following years, Kawashima *et al.*[5,6] confirmed the linear equilibrium geometry of HBO using microwave spectroscopy. They also provided vibrational frequencies and rotational spectra of gas-phase HBO.

Theoretically, several studies were carried out to calculate the equilibrium geometry and dipole moment of HBO.[9–15] Summers and Tyrrell 9 determined that the linear $^1\Sigma^+$ HBO isomer was the global minimum by Hartree–Fock calculations. Zyubina *et al.*[10] reported the potential energy surface (PES) and minimum energy path (MEP) of the isomerization from HBO to BOH and determined the equilibrium geometries of HBO and its isomer BOH. Jr *et al.*[11] determined the geometries, physical properties and energetics of the HBO–BOH system with self-consistent-field (SCF), configuration interaction (CI), and coupled cluster (CC) levels of theory. Later, Gole and Michels[12] constructed the PESs for X ^{1}A′ and A ^{3}A′ states of the HBO–BOH system and provided a more detailed characterization of the PESs. Ha and Makarewicz[13] reported the first two-dimensional PES of HBO using the second-order Møller–Plesset perturbation theory with the aug-cc-pVTZ basis set and two local minima were found in this PES. Peng *et al.*[14] constructed three PESs for ^{1}A′, ^{3}A′ and ^{3}A″ states of HBO using the multireference perturbation theory with the cc-pVTZ(6d,10f) basis set and expounded the interconversion pathways from BOH to HBO based on these PESs. Recently, DeYonker *et al.*[15] investigated the equilibrium structures and physical properties of 18 electronic states for HBO, BOH and their bent counterparts. They also provided the first consistent set of predictions for the singlet excited electronic states of HBO and BOH.

Previous experimental studies only investigated the HBO in the laboratory and no experiments have been reported to detect HBO in astronomical environments so far. Besides, all theoretical studies mentioned above mainly focused on the specific geometries and energies of HBO. Thus, this work aims to present a first and comprehensive molecular line list for the ground electronic state X ^{1}A′ of HBO. First of all, we reported the accurate PES and dipole moment surface (DMS) of the

School of Energy and Power Engineering, Shandong University, 27 Shanda Nanlu, Jinan, 250061, PR China. E-mail: liulinhua@sdu.edu.cn, z.qin@sdu.edu.cn

† Electronic supplementary information (ESI) available: Supplementary data include the coefficients of the HBO PES and DMS, and the explanation of the vibrational quantum numbers. See DOI: https://doi.org/10.1039/d3cp05997a

ground state HBO ($X\ ^1A'$), which were constructed based on the high-quality *ab initio* points. Second, a molecular line list of HBO is computed based on the obtained PES and DMS. This newly computed line list covers infrared wavelengths $\lambda \geq 1.11$ μm (0–9000 cm^{-1}), and is suitable for temperatures up to $T = 3000$ K. The line list of HBO contains over 74 797 464 transitions between 435 631 states with rotational excitation up to $J = 120$, where J is the total angular momentum quantum number of the molecule.

This work is organised as follows. Section 2 presents the details of constructing the PES, DMS and the variational calculations used to produce the line list. Results are discussed in Section 3, including the evaluation of the line list and temperature-dependent partition function. Finally, conclusions are drawn in Section 4.

2 Methods

Generating a molecular line list for HBO requires the PES, DMS, and variational nuclear motion program.[16] In this work, all *ab initio* calculations were performed with the MOLPRO 2015 package[17] and the variational calculations used the nuclear motion program TROVE.[18–21] The details of the three parts are described in the following subsections. The coordinates used to generate the PES and DMS are shown in Fig. 1.

2.1 Potential energy surface

The PES of the ground state HBO was computed using the explicitly correlated coupled cluster method CCSD(T)-F12b[22] with all electrons correlated. The ground state of HBO contains fourteen electrons, including one electron from hydrogen, five electrons from boron, and eight electrons from oxygen. The augmented correlation-consistent basis set included core–valence electron correlation and scalar relativistic effects (aug-cc-pwCVQZ-DK)[23] is used for all atoms. A total of 28 524 *ab initio* points with energies up to $hc{\cdot}30\,000$ cm^{-1} (h is the Planck constant and c is the speed of light) were calculated to construct the PES. The grid points around the equilibrium geometry were generated to be dense enough to ensure an adequate description of this region. The *ab initio* potential energy points were distributed in three internal structure coordinates. For energies below $hc{\cdot}30\,000$ cm^{-1}, the bond length B–H is $1.60 \leq r_{BH} \leq 3.35a_0$, the bond length B–O is $1.85 \leq r_{BO} \leq 2.95a_0$, the interbond angle is $90^\circ \leq \theta_{HBO} \leq 180^\circ$, and the bond length interval is $0.05a_0$. For energies below $hc{\cdot}17\,000$ cm^{-1}, the bond length B–H is $1.65 \leq r_{BH} \leq 3.3a_0$, the bond length B–O is $1.95 \leq r_{BO} \leq 2.8a_0$, the interbond angle is $100^\circ \leq \theta_{HBO} \leq 180^\circ$, and the bond length interval is $0.02a_0$.

The three coordinates of the PES are expressed as follows:

$$y_1 = 1 - \exp(-a(r_1 - r_1^e)), \quad (1)$$

$$y_2 = 1 - \exp(-b(r_2 - r_2^e)), \quad (2)$$

$$y_3 = \cos\theta - \cos\theta_e, \quad (3)$$

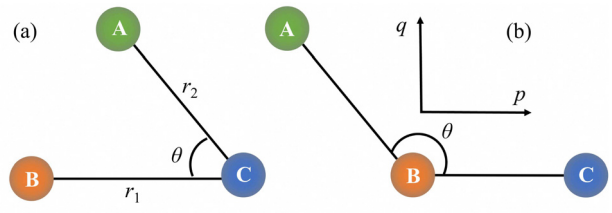

Fig. 1 (a) The coordinates used to generate the PES. (b) The coordinates used to generate the DMS.

where r_1 and r_2 are the bond lengths of B–H and B–O, θ is the interbond angle ∠(H–B–O), a and b are the Morse parameters ($a = 0.8$ $Å^{-1}$, $b = 0.6$ $Å^{-1}$), and r_1^e, r_2^e and θ_e are the equilibrium parameters ($r_1^e = 2.2093a_0$, $r_2^e = 2.2767a_0$, and $\theta_e = 180^\circ$). The PES is represented using the following form ref. 24:

$$V = \sum_{i_1,i_2,i_3} c_{i_1,i_2,i_3} y_1^{i_1} y_2^{i_2} y_3^{i_3} + F, \quad (4)$$

$$F = d_1 \exp(-h_1 r_{OH}) + d_2 \exp(-h_2 r_{OH}^2), \quad (5)$$

$$r_{OH} = \sqrt{r_1^2 + r_1^2 - 2r_1 r_2 \cos\theta}, \quad (6)$$

where the $i_1 + i_2 + i_3 \leq 6$, the function F is to ensure the PES behaves reasonably when the O and H atoms get closer. The parameters d_1, d_2, h_1 and h_2 have values of 5×10^5 cm^{-1}, 5×10^4 cm^{-1}, 15 $Å^{-1}$ and 10 $Å^{-1}$, respectively.

The expansion coefficients c_{i_1,i_2,i_3} in eqn (4) are determined through the weighted least-squares fitting to the *ab initio* data. The fitting weights w_i are employed in the fitting process to favour energies below 1.5×10^4 cm^{-1} and use the following form ref. 25:

$$w_i = \left(\frac{\tanh\left[-6 \times 10^{-4}\left(E_i - 1.5 \times 10^4\right) + 1.002002002\right]}{2.002002002}\right) \times \frac{1}{NE_i^{(w)}}, \quad (7)$$

where E_i is the ith geometry's potential energy, $E_i^{(w)} = \max(E_i, 1 \times 10^4)$ and $N = 1 \times 10^4$ cm^{-1}. The weighted root-mean-square deviation (rmsd) is 0.07 743 cm^{-1}. These coefficients of the analytical PES of HBO are provided in the ESI.†

2.2 Dipole moment surface

The DMS of HBO was computed on the same grid of nuclear geometries used to compute the PES at the CCSD(T)-F12b/aug-cc-pVQZ[26] level of theory for all atoms. The resolution of the identity OptRI basis[27] was utilized for the auxiliary basis sets (ABS) with a Slater geminal exponent value of $\beta = 1.4a_0^{-1}$. For density fitting, the aug-cc-pV5Z/JKFIT[28] and aug-cc-pwCV5Z/MP2FIT[29] basis sets were employed. The dipole moment vector $\boldsymbol{\mu}$ was represented by the pq axis system.[30] In this system, the origin is fixed at the B atom, and the p axis is along the r_{BO} bond with the q axis perpendicular to the p axis. To determine the dipole moment components $\boldsymbol{\mu}_p$ and $\boldsymbol{\mu}_q$, the central finite differences were utilised, in which an external electric field with components ± 0.005 a.u. was applied along the p and q axis.

The $\boldsymbol{\mu}_p$ and $\boldsymbol{\mu}_q$ components were expressed as the following forms:

$$\mu_p = \sum_{i_1,i_2,i_3} C^p_{i_1,i_2,i_3} \phi_1^{i_1} \phi_2^{i_2} \phi_3^{i_3}, \quad (8)$$

$$\mu_q = \sin(\pi - \theta) \sum_{i_1,i_2,i_3} C^q_{i_1,i_2,i_3} \phi_1^{i_1} \phi_2^{i_2} \phi_3^{i_3}, \quad (9)$$

with the coordinates

$$\phi_1 = r_1 - r_1^e, \quad (10)$$

$$\phi_2 = r_2 - r_2^e, \quad (11)$$

$$\phi_3 = \cos\theta - \cos\theta_e, \quad (12)$$

where the maximum expansion orders $i_1 + i_2 + i_3$ are 6 and 5 for $\boldsymbol{\mu}_p$ and $\boldsymbol{\mu}_q$, respectively. r_1^e, r_2^e and θ_e are the same as those of the HBO PES. Using the same weight factors as given in eqn (7), the total weighted rmsds for $\boldsymbol{\mu}_p$ and $\boldsymbol{\mu}_q$ components are 0.00 012 and 0.0 002 Debye, respectively. The coefficients of the analytical HBO DMS are provided in the ESI.†

2.3 Line list calculations

Line list calculations employ the nuclear motion program TROVE[20,21] and details of TROVE have been discussed extensively in previous works.[19,31–33]

During the calculation in TROVE, the potential energy operator and the exact kinetic energy operator are represented by a sixth-order power series expansion and a fourth-order power series expansion, respectively. For the three vibrational modes, each 1D Hamiltonian operator is obtained with all other degrees of freedom frozen at their equilibrium values. Large symmetry-adopted basis sets are also used to ensure convergence. Two primitive stretching basis functions ϕ_{n_1} and ϕ_{n_2} are obtained with the Numerov–Cooley method[34,35] on a grid of 2000 and 3000 points to solve the 1D Schrödinger equations, respectively. The primitive bending basis function ϕ_{n_3} is constructed using associated Laguerre polynomials on a grid of 6000 points to solve the 1D Schrödinger equation, where L is the vibrational angular momentum quantum number.

The zero-point energy of HBO was computed to be 3097.506 cm^{-1}. Rovibrational energy levels, transitions and Einstein A coefficients of the ground state HBO are computed in the 0–9000 cm^{-1} range (above the zero-point energy) with a lower state energy threshold of hc·15 000 cm^{-1}. Finally, a total of 142 038 890 transitions between 195 970 energy levels were computed with the values of J up to 120.

3 Results

3.1 Line list format

The ExoMol database (**https://www.exomol.com**) has become the go-to place for data on hot molecules for studies of exoplanets and provides an important service to the astronomical community. As standard, we provide the line list of HBO in the ExoMol data format[36] as two file types. To determine the quantum numbers and molecular symmetry of HBO, the rovibronic energy levels and wavefunction are classified under the C_s(M)[37] molecular symmetry group. Table 1 gives an example of the **.states** file, which contains part obtained vibrational energy levels (in cm^{-1}) and their unique state counting numbers, total state degeneracy, total angular momentum, symmetry, quantum number labelling (symmetric stretching ν_1, bending ν_2, antisymmetric stretching ν_3 and vibrational angular momentum quantum number L), contribution C_i from the largest eigencoefficient used to assign the rovibrational state, and the vibrational quantum numbers used in TROVE (n_1, n_2 and n_3). For the fundamental ν_2 and ν_3 frequency, our computed results have the values of 753.71 and 1815.82 cm^{-1}, which compares well with the experimental values[5] of 754 and 1826 cm^{-1}, respectively. For the symmetric stretching mode ν_1, there has been some debate in the literature[5,8] with differing values presented. Lory and Porter[8] reported an experimental value of 2849 ± 10 cm^{-1}, but Kawashima *et al.*[5] reported a rather lower harmonic ω_1 value of 2821 cm^{-1}. Despite not being in complete agreement with these estimated values, we are confident that our calculated fundamental wavenumber of ν_1 2786.85 cm^{-1} is closer to the true value based on the *ab initio* theory used in this work. Table 2 shows the example of the **.trans** file and it contains all computed transitions with upper and lower state counting numbers and Einstein A coefficients (in s^{-1}).

Table 1 Extract from the **.states** file of the HBO line list

n^a	E^b	$g_{tot}{}^c$	J^d	$G_{tot}{}^e$	$\nu_1{}^f$	$\nu_2{}^{lin\,g}$	$\nu_3{}^h$	L^i	$C_i{}^j$	$n_1{}^k$	$n_2{}^k$	$n_3{}^k$
1	0.000000	8	0	A′	0	0	0	0	1.00	0	0	0
2	1487.187414	8	0	A′	0	2	0	0	1.00	0	0	1
3	1815.819307	8	0	A′	0	0	1	0	1.00	1	0	0
4	2786.850870	8	0	A′	1	0	0	0	1.00	0	1	0
5	2949.648434	8	0	A′	0	4	0	0	1.00	0	0	2
6	3308.438531	8	0	A′	0	2	1	0	1.00	1	0	1
7	3615.679294	8	0	A′	0	0	2	0	1.00	2	0	0
8	4241.771257	8	0	A′	1	2	0	0	1.00	0	1	1
9	4389.315208	8	0	A′	0	6	0	0	1.00	0	0	3
10	4591.155279	8	0	A′	1	0	1	0	1.00	1	1	0

[a] State counting number. [b] State energy (in cm^{-1}). [c] Total state degeneracy. [d] Total angular momentum quantum number. [e] Overall symmetry in C_s(M) (A′ or A″). [f] Symmetric stretching ν_1 mode vibrational quantum number. [g] Linear molecule bending ν_2 mode vibrational quantum number. [h] Antisymmetric stretching ν_3 mode vibrational quantum number. [i] Vibrational angular momentum quantum number $L = |l|$ associated with ν_2 mode. [j] Largest coefficient used in the TROVE assignment. [k] TROVE vibrational quantum numbers.

Table 2 Extract from the **.trans** file for the 0–100 cm^{-1} window of the HBO line list

f^a	i^b	$A_{fi}{}^c$
12 086	11 290	2.87588961 × 10^{-7}
5644	3002	3.08141173 × 10^{-8}
14 815	11 283	4.92476732 × 10^{-7}
8470	6183	2.50773228 × 10^{-7}
19 751	17 932	3.14723674 × 10^{-6}
28 207	26 398	3.30527574 × 10^{-6}
22 572	20 636	2.73468246 × 10^{-6}
17 934	14 111	1.69918048 × 10^{-6}
29 470	25 391	7.81900111 × 10^{-6}
28 216	29 467	1.51217508 × 10^{-6}

[a] Upper state counting number. [b] Lower state counting number. [c] Einstein A coefficient (in s^{-1}).

3.2 Temperature-dependent partition functions

The temperature-dependent partition function is defined as:

$$Q(T) = \sum_i g_{\mathrm{tot}} \exp\left(\frac{-E_i}{k_{\mathrm{B}}T}\right), \quad (13)$$

$$g_{\mathrm{tot}} = g_{\mathrm{ns}}(2J_i + 1), \quad (14)$$

where E_i and J_i are the energy and total angular momentum quantum number of the unique state i, respectively. g_{ns} is the nuclear spin statistical weight for HBO with a value of 8, k_{B} is the Boltzmann constant, and T is the absolute temperature in K. $Q(T)$ is obtained by summing overall computed rovibrational energy levels on a 1 K grid in the range of 1–3000 K.

Fig. 2 illustrates the convergence of $Q(T)$ as a function of J for different temperatures. The values of J have little effect on $Q(T)$ for temperatures below 500 K, but $Q(T)$ changes dramatically with the increase in temperature. When temperatures are above 2000 K, a significant number of J states have to be considered in the summation of eqn (13), and the value of Q (3000 K) is converged to 0.002 per cent for HBO at J = 120. Our obtained value of Q (300 K) is 169.8953, which is much larger than that of 159.7938 from the cologne database for molecular spectroscopy (CDMS).[38–40] This is because the value from CDMS only considers the ground vibrational state. However, the low-lying rovibrational states of the ground state HBO should also be properly considered.[16] As the line list is computed with a lower state energy threshold of hc·15 000 cm^{-1}, it is necessary to calculate the reduced partition function $Q_{\mathrm{red}}(T)$, which only contains energy levels up to the energy threshold in the summation of eqn (13). The ratio of $Q_{\mathrm{red}}(T)/Q(T)$ is plotted in Fig. 3. The value of the $Q_{\mathrm{red}}(T)/Q(T)$ is about 1 for temperatures below 1000 K, which indicates that the completeness of the line list is not altered by the lower state energy threshold at low temperatures as the line list determines the partition function. The ratio of $Q_{\mathrm{red}}(T)/Q(T)$ begins to decrease at about 1500 K and reaches about 0.95 at 3000 K. Therefore, the $Q(T)$ can be regarded as converged at T = 3000 K. With the ratio of $Q_{\mathrm{red}}(T)/Q(T)$ decreasing, using the line list may lead to a progressive loss of opacity. The missing opacity contribution can be estimated from $Q_{\mathrm{red}}(T)/Q(T)$ if needed.[41]

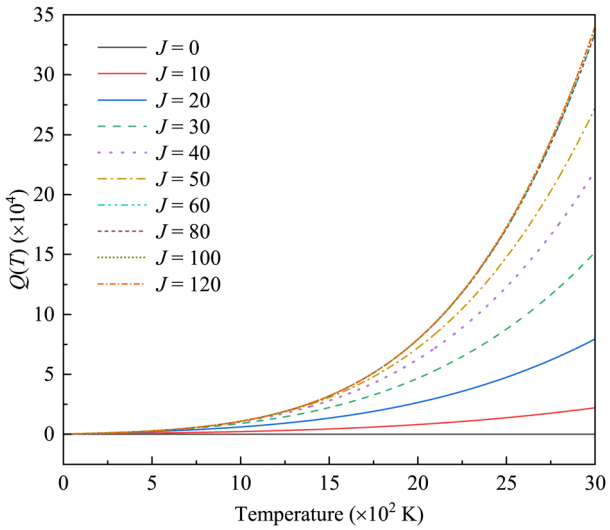

Fig. 2 Convergence of the temperature-dependent partition function $Q(T)$ of HBO with respect to the total angular momentum quantum number J.

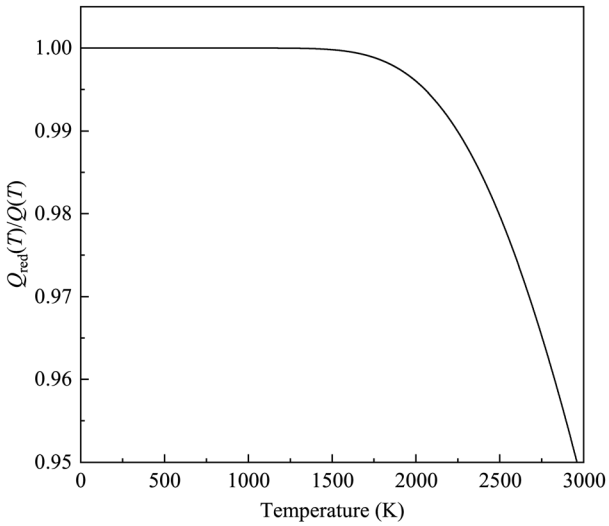

Fig. 3 The ratio of Q_{red}/Q as a function of temperature for HBO.

3.3 Simulated spectra

The EXOCROSS program[42] is used to carry out the spectral simulations of HBO. An overview of the spectrum of HBO is shown in Fig. 4. The temperature-dependent absorption cross-sections are simulated at a resolution of 1 cm^{-1} using a Gaussian line profile with a half width at half maximum (HWHM) of 1 cm^{-1}. Notably, the spectrum gets smoother and flatter with the increase of the temperature. This is because the population of vibrationally excited states is increased as the temperature rises, leading to the rotational bands to broaden significantly.

The absolute line intensities were calculated by,

$$I(f \leftarrow i) = \frac{A_{fi}}{8\pi c} g_{\mathrm{ns}}(2J_f + 1) \frac{\exp(-E_i/k_{\mathrm{B}}T)}{Q(T)\nu_f^2}\left[1 - \exp\left(-\frac{hc\nu_{fi}}{k_{\mathrm{B}}T}\right)\right], \quad (15)$$

where i and f are the initial and final state counting numbers, respectively. E_i is the energy of state i, J_f is the total angular momentum quantum number of state f. A_{fi} is the Einstein A coefficient of a transition with wavenumber ν_{fi} (in cm^{-1}) between state i and f. h is the Planck constant and c is the speed of light.

Fig. 5 shows the computed HBO stick spectrum against the data from CDMS. The data of CDMS contains 43 lines up to J = 43 based on the observed transitions from Kawashima *et al.*[6] and the CDMS line intensities are based on the calculated electric dipole moment value of 2.692 Debye in the ground state.[15] Our calculated electric dipole moment is 2.752 Debye,

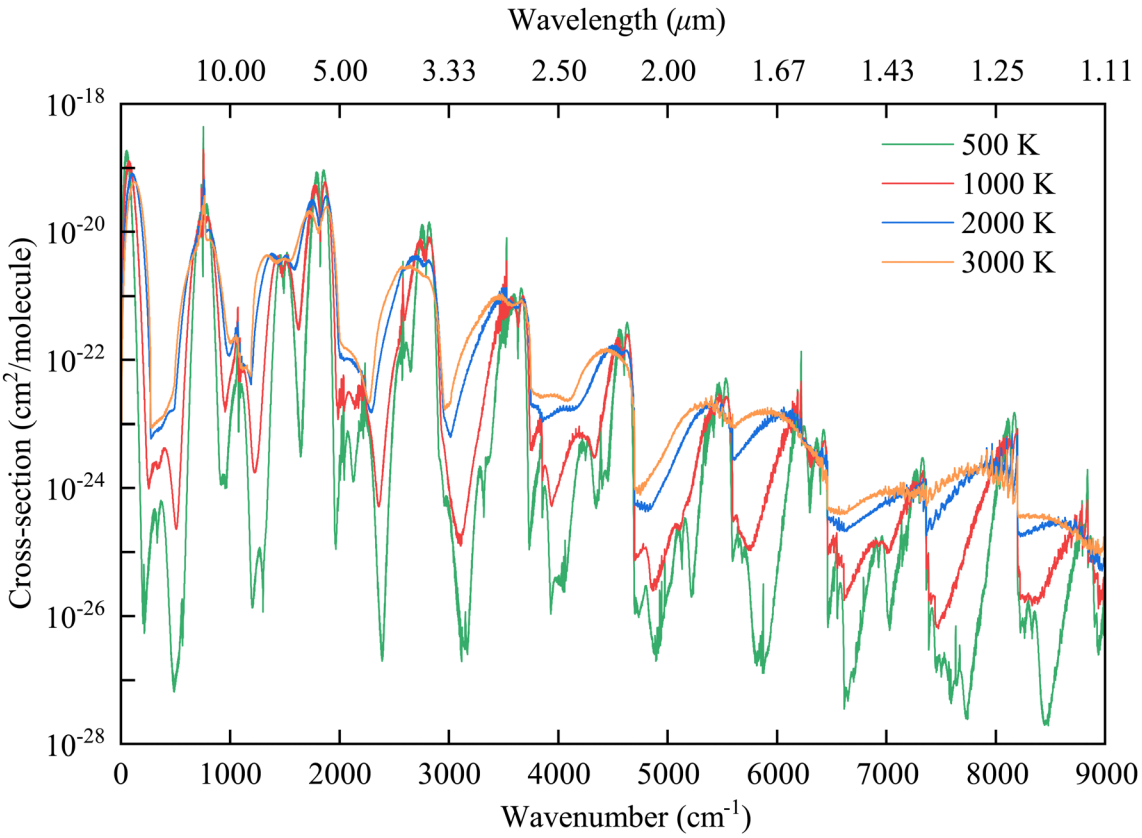

Fig. 4 Temperature (in K) dependence of the spectrum of HBO. Absorption cross sections were computed at a resolution of 1 cm^{-1} with a Gaussian line profile with a half-width at half-maximum (HWHM) of 1 cm^{-1}.

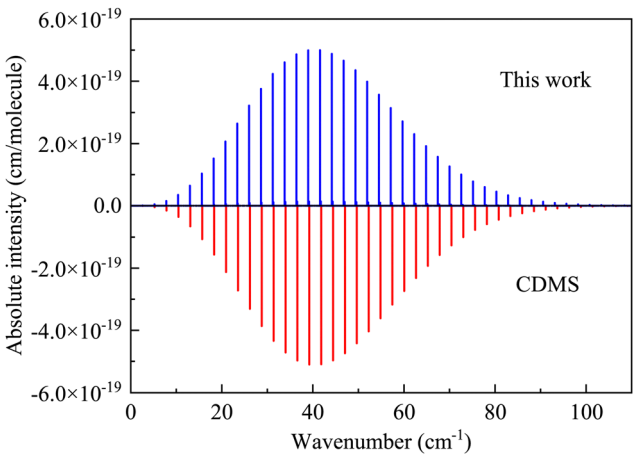

Fig. 5 Comparison of the computed stick spectrum of HBO with all transition data from the CDMS[38–40] at T = 300 K.

which is slightly bigger than the value used by CDMS. The lack of high-resolution spectroscopic measurements makes it difficult to improve the accuracy of our calculated line list with laboratory measurements, our entirely calculated line list still show good agreement with the CDMS one. The deviations between our computed wavenumbers and the observed CDMS wavenumbers are within 0.69 cm^{-1}. Overall band shape is reproduced well with our computed HBO line list, both in terms of wavenumber and intensity. Due to the available experimental intensity information is obtained at room temperature, its difficult to quantify the accuracy of the computed line intensities at high temperatures. Previous *ab initio* DMSs[16,33] with similar levels of theory suggest that our HBO transition intensities can be well within 5–10 per cent of experimentally determined values.

4 Conclusion

For the first time, we report a comprehensive molecular line list for HBO. The HBO line list covers the 0–9000 cm^{-1} range (wavelengths $\lambda \geq 1.11$ μm) for states below J = 120 and is applicable for temperatures up to 3000 K. The line list is constructed using the TROVE nuclear motion code based on the purely *ab initio* PES and DMS. As the deviations between the computed and observed wavenumbers are within 0.03 cm^{-1}, our line list shows good agreement with the experimentally derived microwave data given by CDMS at room temperature. Due to the lack of experimental spectroscopic data at high temperatures to improve the accuracy of the computed line list, the current line list for the highly excited states or shorter wavelengths is not accurate enough. Our line list is the first available data for predicting spectra of HBO at temperatures above room temperature and can be used to identify the

possible transitions of HBO in exoplanet and brown dwarf atmospheres.

Data availability

Data available on request from the authors.

Conflicts of interest

There are no conflicts to declare.

Acknowledgements

We thank Jonathan Tennyson, Sergei N. Yurchenko, Alec Owens and Guangan Chen for their help with the TROVE calculations. This work was financed by the National Natural Science Foundation of China (Grant no. 52106098, 52076123), the Natural Science Foundation of Shandong Province (Grant no. ZR2021QE021) and the Young Scholars Program of Shandong University. The scientific calculations in this paper have been done on the HPC Cloud Platform of Shandong University.

Notes and references

1 Y. V. Voronov, S. A. Yakovleva and A. K. Belyaev, *Mon. Not. R. Astron. Soc.*, 2023, **520**, 107–112.
2 A. M. Boesgaard, M. G. Lum, C. P. Deliyannis, J. R. King, M. H. Pinsonneault and G. Somers, *Astrophys. J.*, 2016, **830**, 49.
3 S. Randich and L. Magrini, *Front. Astron. Space Sci.*, 2021, **8**, 616201.
4 M. Agúndez, J. Martnez, P. de Andres, J. Cernicharo and J. A. Martn-Gago, *Astron. Astrophys.*, 2020, **637**, A59.
5 Y. Kawashima, Y. Endo and E. Hirota, *J. Mol. Spectrosc.*, 1989, **133**, 116–127.
6 Y. Kawashima, Y. Endo, K. Kawaguchi and E. Hirota, *Chem. Phys. Lett.*, 1987, **135**, 441–445.
7 Y. Kawashima, K. Kawaguchi and E. Hirota, *Chem. Phys. Lett.*, 1986, **131**, 205–208.
8 E. R. Lory and R. F. Porter, *J. Am. Chem. Soc.*, 1971, **93**, 6301–6302.
9 N. L. Summers and J. Tyrrell, *J. Am. Chem. Soc.*, 1977, **99**, 3960–3965.
10 T. Zyubina, O. Charkin and L. Gurvich, *J. Struct. Chem.*, 1979, **20**, 1–7.
11 C. A. Richards Jr, G. Vacek, B. J. DeLeeuw, Y. Yamaguchi and H. F. Schaefer III, *J. Chem. Phys.*, 1995, **102**, 1280–1287.
12 J. Gole and H. Michels, *J. Chem. Phys.*, 1995, **103**, 7844–7850.
13 T.-K. Ha and J. Makarewicz, *Chem. Phys. Lett.*, 1999, **299**, 637–642.
14 Q. Peng, Y. Wang, B. Suo, Q. Shi and Z. Wen, *J. Chem. Phys.*, 2004, **121**, 778–782.
15 N. J. DeYonker, S. Li, Y. Yamaguchi, H. F. Schaefer, T. D. Crawford, R. A. King and K. A. Peterson, *J. Chem. Phys.*, 2005, **122**, 234316.
16 A. Owens, S. O. Wright, Y. Pavlenko, A. Mitrushchenkov, J. Koput, S. N. Yurchenko and J. Tennyson, *Mon. Not. R. Astron. Soc.*, 2024, **527**, 731–738.
17 H. J. Werner, P. J. Knowles and G. Knizia, *et al.*, *MOLPRO, version 2015.1, a package of ab initio programs*, **https://www.molpro.net**.
18 S. N. Yurchenko and T. M. Mellor, *J. Chem. Phys.*, 2020, **153**, 154106.
19 S. N. Yurchenko, A. Yachmenev and R. I. Ovsyannikov, *J. Chem. Theor. Comput.*, 2017, **13**, 4368–4381.
20 J. Tennyson and S. N. Yurchenko, *Int. J. Quantum Chem.*, 2017, **117**, 92–103.
21 S. N. Yurchenko, W. Thiel and P. Jensen, *J. Mol. Spectrosc.*, 2007, **245**, 126–140.
22 T. B. Adler, G. Knizia and H.-J. Werner, *J. Chem. Phys.*, 2007, **127**, 221106.
23 W. A. De Jong, R. J. Harrison and D. A. Dixon, *J. Chem. Phys.*, 2001, **114**, 48–53.
24 V. G. Tyuterev, S. A. Tashkun and D. W. Schwenke, *Chem. Phys. Lett.*, 2001, **348**, 223–234.
25 H. Partridge and D. W. Schwenke, *J. Chem. Phys.*, 1997, **106**, 4618–4639.
26 R. A. Kendall, T. H. Dunning Jr and R. J. Harrison, *J. Chem. Phys.*, 1992, **96**, 6796–6806.
27 K. E. Yousaf and K. A. Peterson, *J. Chem. Phys.*, 2008, **129**, 184108.
28 F. Weigend, *Phys. Chem. Chem. Phys.*, 2002, **4**, 4285–4291.
29 C. Hättig, *Phys. Chem. Chem. Phys.*, 2005, **7**, 59–66.
30 U. Jorgensen and P. Jensen, *J. Mol. Spectrosc.*, 1993, **161**, 219–242.
31 S. N. Yurchenko, R. J. Barber, A. Yachmenev, W. Thiel, P. Jensen and J. Tennyson, *J. Phys. Chem. A*, 2009, **113**, 11845–11855.
32 A. Yachmenev and S. N. Yurchenko, *J. Chem. Phys.*, 2015, **143**, 014105.
33 A. Owens, J. Tennyson and S. Yurchenko, *Mon. Not. R. Astron. Soc.*, 2021, **502**, 1128–1135.
34 B. Noumerov, *Mon. Not. R. Astron. Soc.*, 1924, **84**, 592.
35 J. Cooley, *Math. Comput.*, 1961, **15**, 363–374.
36 J. Tennyson, S. N. Yurchenko, A. F. Al-Refaie, V. H. Clark, K. L. Chubb, E. K. Conway, A. Dewan, M. N. Gorman, C. Hill and A. Lynas-Gray, *et al.*, *J. Quant. Spectrosc. Radiat. Transfer*, 2020, **255**, 107228.
37 P. R. Bunker and P. Jensen, *Molecular symmetry and spectroscopy*, NRC Research Press, Ottawa, 2006, vol. 46853.
38 H. S. Müller, S. Thorwirth, D. Roth and G. Winnewisser, *Astron. Astrophys.*, 2001, **370**, L49–L52.
39 H. S. Müller, F. Schlöder, J. Stutzki and G. Winnewisser, *J. Mol. Struct.*, 2005, **742**, 215–227.
40 C. P. Endres, S. Schlemmer, P. Schilke, J. Stutzki and H. S. Müller, *J. Mol. Spectrosc.*, 2016, **327**, 95–104.
41 L. Neale, S. Miller and J. Tennyson, *Astrophys. J.*, 1996, **464**, 516–520.
42 S. N. Yurchenko, A. F. Al-Refaie and J. Tennyson, *Astron. Astrophys.*, 2018, **614**, A131.